Climate Dynamics (2022) 59:3287–3304
https://doi.org/10.1007/s00382-022-06261-w

ENSO teleconnections and atmospheric mean state in idealised simulations

Emanuele Di Carlo[1,2] · Paolo Ruggieri[2] · Paolo Davini[3] · Stefano Tibaldi[4] · Susanna Corti[1]

Received: 11 August 2021 / Accepted: 12 March 2022 / Published online: 13 April 2022

Abstract
Understanding the natural and forced variability of the general circulation of the atmosphere and its drivers is one of the grand challenges in climate science. In particular, it is of paramount importance to understand to what extent the systematic error of global climate models affects the processes driving such variability. This is done by performing a set of simulations (ROCK experiments) with an intermediate complexity atmospheric model (SPEEDY), in which the Rocky Mountains orography is modified (increased or decreased) to influence the structure of the North Pacific jet stream. For each of these modified-orography experiments, the climatic response to idealized sea surface temperature (SST) anomalies of varying intensity in the El Niño Southern Oscillation (ENSO) region is studied. ROCK experiments are characterized by variations in the Pacific jet stream intensity whose extension encompasses the spread of the systematic error found in state-of-the-art climate models. When forced with ENSO-like idealised anomalies, they exhibit a non-negligible sensitivity in the response pattern over the Pacific North American region, indicating that a change/bias in the model mean state can affect the model response to ENSO. It is found that the classical Rossby wave train response generated by ENSO is more meridionally oriented when the Pacific jet stream is weaker, while it exhibits a more zonal structure when the jet is stronger. Rossby wave linear theory, used here to interpret the results, suggests that a stronger jet implies a stronger waveguide, which traps Rossby waves at a lower latitude, favouring a more zonally oriented propagation of the tropically induced Rossby waves. The shape of the dynamical response to ENSO, determined by changes in the intensity of the Pacific Jet, affects in turn the ENSO impacts on surface temperature and precipitation over Central and North America. Furthermore, a comparison of the SPEEDY results with CMIP6 models behaviour suggests a wider applicability of the results to more resources-demanding, complete climate GCMs, opening up to future works focusing on the relationship between Pacific jet misrepresentation and response to external forcing in fully-fledged GCMs.

Keywords Climate sensitivity · ENSO teleconnections · Atmospheric mean state · Rossby waves · Jet stream

1 Introduction

State-of-the-art climate models still exhibit non-negligible biases in simulating the main features of the extratropical circulation, as can be seen from the results of the successive Climate Model Intercomparison Projects (CMIP3-5-6) (e.g., Meehl et al. 2007, Ulbrich et al. 2009, Taylor et al. 2012, Mizuta 2012, Zappa et al. 2013, Chang 2013, Shaffrey and Hodges 2013, Eyring et al. 2016, Harvey et al. 2020). It is therefore of critical importance to understand to what extent the processes driving the variability of the mid-latitude atmospheric circulation are affected by model systematic errors.

One of the main drivers of both tropical and extratropical variability is the El Niño-Southern Oscillation (ENSO) (Philander 1990, Wang 2017), which generates global teleconnections in both the atmosphere and the ocean. ENSO is a quasi-periodic, coupled ocean-atmosphere phenomenon characterized by fluctuations of the sea surface temperature

✉ Emanuele Di Carlo
emanuele.dicarlo3@unibo.it

1 CNR Institute of Atmospheric Sciences and Climate, Bologna, Italy

2 University of Bologna, Bologna, Italy

3 CNR Institute of Atmospheric Sciences and Climate, Torino, Italy

4 Fondazione CentroEuro-Mediterraneo sui Cambiamenti Climatici, Bologna, Italy

(SST), thermocline depth, and sea level pressure (SLP) across the equatorial Pacific. The state of the Tropical Pacific climate with respect to ENSO can be synthetically described as being in one of three conditions: Neutral, El Niño, and La Niña. El Niño is the positive phase of ENSO (associated with a warm SST anomaly) while La Niña is its negative phase (with a cold SST anomaly).

One of the main atmospheric consequences of ENSO is the rearrangement of the atmospheric Walker Circulation which leads to a longitudinal shift of the associated convective rainfall patterns (Dai and Wingley 2000). During an El Niño event, the warm SST anomaly, and the related anomalous convection in the eastern Tropical Pacific lead to an increased atmospheric low-level convergence and a corresponding upper-tropospheric divergence, generating an anomalous vorticity source in the tropics. The upper-level component of this vorticity source acts as a Rossby Wave Source (RWS) (Hoskins and Karoli 1981). This RWS, in turn, sets off a Rossby Wave train that tends to propagate upward, northward, and eastward in the North Pacific, modulating the intensity of the Aleutian Low and causing teleconnections patterns in the extratropics (Trenberth et al. 1998). Such Rossby Wave perturbations propagating from the tropical regions into the midlatitudes constitute a sort of atmospheric bridge which can spread the signature of ENSO all over the globe (Trenberth et al. 1998).

During the positive ENSO phase, a deeper Aleutian Low can also generate upward propagating waves that can reach the stratosphere and weaken the stratospheric polar vortex. During events associated with a strong weakening of the polar vortex, anomalies can propagate back downward into the troposphere and project onto the North Atlantic (Cagnazzo and Manzini 2009, Butler et al. 2014). During La Niña events, the response is broadly of the opposite sign, but weaker (Jiménez–Esteve and Domeisen 2018). Several studies showed that the winter response to ENSO, on the North Atlantic, changes from the early winter (November-December) to the late winter (January-March)(Moron and Gouirand 2003, King et al. 2021). The early winter teleconnection resembles the East Atlantic pattern, while the late winter teleconnection projects onto the NAO pattern (King et al. 2018, Mezzina et al. 2020). This difference in the response patterns is due to distinct propagation pathways; the early winter response involves a tropospheric pathway, while the late winter response involves both the tropospheric and stratospheric pathways (Ayarzagüena et al. 2018, Domeisen et al. 2019).

In the Pacific region, ENSO can shift the subtropical Pacific jet stream over the western coast of North America, influencing the weather and climate over Mexico, United States and Canada (Seager et al. 2005a,b). During El Niño (La Niña) events, the southern part of North America is usually colder (warmer) and wetter (dryer), while the northwestern part is mostly warmer (colder) and dryer (wetter). A consensus has not been reached on whether ENSO or the natural atmospheric variability modulate the climate over the western coast of North America (Lopez and Kirtman 2019). There is also an ongoing debate regarding the connection between ENSO and the Pacific North American pattern (PNA). PNA is a characteristic pattern of the Northern Hemisphere internal variability, that includes four main centers of action observed in the 200 hPa geopotential height (Wallace and Gutzler 1981) and has significant influence on temperature and precipitation over North America (Gershunov and Cayan 2003). Some authors argue that ENSO can only amplify internal variability and cannot generate new patterns (Molteni et al. 1993, Lau 1997, Blade 1999, Palmer 1999). Straus and Shukla (2002), on the other hand, suggest that the external forcing (i.e., ENSO) can lead to patterns that are different from those typical of the internal variability. Lopez and Kirtman (2019) found that ENSO produces response patterns over North America which are different from those of PNA. Considering the limited observational record, the ENSO signal is difficult to disentangle from the internal variability patterns.

The role of global climate model biases in modulating the atmospheric response to ENSO is also to this day rather unclear, with contrasting conclusions achieved by different authors. Dawson et al. (2011) found that an increase in model resolution to a more realistic mean state, and that a better mean state plays a key role in the propagation of Rossby waves from a tropical source (e.g., El Niño) to the extratropics. Li et al. (2020) show that different model responses to ENSO in the Pacific-North American region and in the North Atlantic region can be explained by differences in the model mean state. Model biases in the North Pacific jet can affect the propagation of Rossby Waves generated in the Tropics, therefore the same RWS can lead to different responses in the Pacific-North American region, depending on the model jet bias. Conversely, they show that the response to El Niño in the North Atlantic and European region is almost independent of the jet bias but can be explained by considering biases in the tropical RWS. Tyrrell and Karpechko (2021) apply a bias correction method to the divergence and temperature tendencies of a general circulation model (GCM) in order to produce several different climatologies, then they apply the ENSO forcing, both positive and negative, for each model climatology. They conclude that there are no significant differences in the responses to ENSO depending on the divergence and temperature tendencies in the troposphere and stratosphere. The climatological bias does not affect the response in the Aleutian Low due to Rossby waves forcing, or the response in the polar vortex due to the upward planetary wave forcing.

Another source of uncertainty related to ENSO forcing and its teleconnections is the impact of the SST bias in state-of-the-art models (Timmermann et al. 2018). Many coupled general circulation models exhibit a cold SST bias in the equatorial Pacific Ocean (reminiscent of a La Niña-like state), which leads to an overly westward displaced rising branch of the Walker Circulation. During an El Niño event, the bias in the convective region leads to a further westward convective response as compared with observations (Bayr et al., 2019a, Domeisen et al., 2015). Since this SST bias is mainly due to the oceanic component of coupled models, climate simulations with prescribed SSTs better represent ENSO teleconnections to the North Pacific and North America (Bayr et al., 2019b).

Considering that investigating the tropical-midlatitude interactions due to ENSO forcing under different model mean states has been shown to be a complex and multifaceted problem, both in observations and in climate GCMs (e.g., the CMIP set of experiments), an intermediate-complexity experimental setup could constitute a fruitful approach. In this work, the attention is therefore focused on a single feature of the model bias: the North Pacific Jet Stream, which is one of the regions where the largest bias and root mean square error (RMSE) are observed in state-of-the-art GCMs, as shown by Fig. 1.

This work aims at exploring how different systematic errors of the Pacific jet stream can affect the model response to ENSO in order to understand to what extent the response of the model to a given forcing changes when the model mean state is modified. This is done by performing several simulations with the atmospheric general circulation model Simplified Parameterizations, primitivE - Equation DYnamics (SPEEDY), forced by climatological SSTs. Each simulation is characterized by a different bias in the Pacific Jet stream, obtained by changing the height of the Rocky Mountains, and an ENSO-forced RWS superimposed on the background flow.

The experimental setup as well as the metrics used are presented in Sect. 2. Results from model simulations are shown in Sect. 3, while in Sect. 4 the results are discussed. Finally, conclusions are drawn in Sect. 5.

2 Materials and methods

2.1 The Model

In the last decades a hierarchy of GCMs has been developed to tackle a wide variety of scientific questions. Starting from the second half of the ’80s, the complexity of GCM has dramatically increased. This has been associated with an increase in computational costs. For academic purposes, however, state-of-the-art GCMs can be too expensive, and here Earth System Models of Intermediate Complexity (EMIC, Claussen, et al. 2002) come into play. These models are sufficiently accurate to be compared with observations, but less complex and computationally cheaper than fully-fledged GCMs.

The model used in this study is an intermediate complexity Atmospheric General Circulation Model developed at the Abdus Salam International Center for Theoretical Physics (ICTP), known as SPEEDY (Simplified parameterization PrimitivE Equation DYnamic (Molteni 2003, Kucharski et al. 2006). Version 41 has been used in the current work. It uses the Held and Suarez hydrostatic spectral dynamical core (Held and Suarez 1994) expressed in the vorticity-divergence form derived by Bourke (1974). A set of parameterizations takes care of processes such as

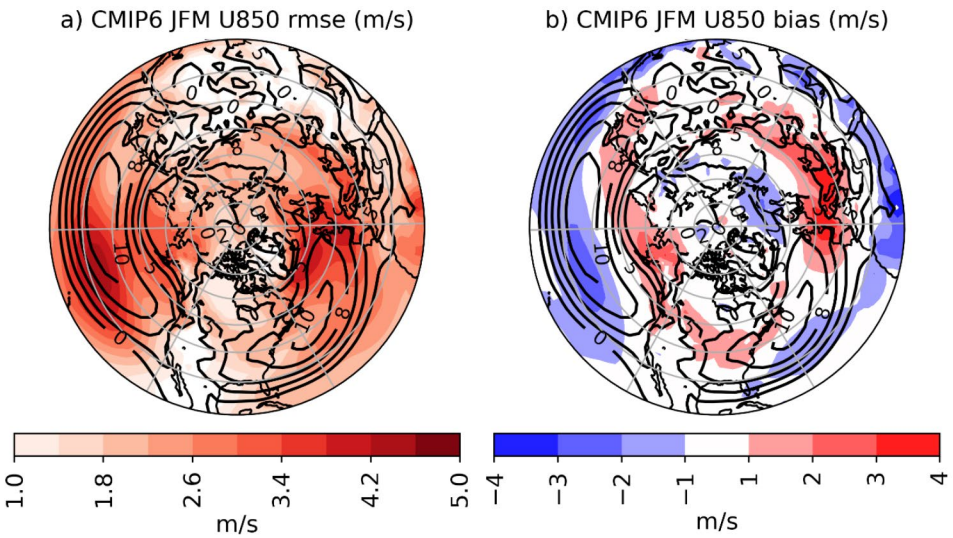

Fig. 1 JFM zonal wind at 850 hPa (a) RMSE (colous) and (b) multi model mean bias (colours) for the CMIP6 atmosphere-only models (AMIP experiment). In both panels, contours are the JFM zonal wind at 850 hPa from ERA-Interim

large-scale condensation, surface fluxes of momentum, vertical diffusion of heat and moisture, convection and short and longwave radiation (Molteni 2003). A one-layer thermodynamic model (Kucharski et al. 2006a, b, 2013a, b) calculates the temperature anomaly for land and sea ice. The horizontal spectral resolution is T30 (~450 Km at the Equator) with 8 vertical levels and an associated regular Gaussian grid of 96×48 points. The SPEEDY model is computationally advantageous, so it can be integrated over centuries at a minor computational cost. Despite the low resolution and the simplified parameterizations, SPEEDY represents satisfactorily several aspects of the atmospheric climate, like the extratropical circulation (Kucharski et al. 2006a, b), planetary-scale variability modes (Molteni et al. 2011), tropical/extratropical teleconnections (Kucharski et al. 2007), ENSO teleconnections in a global warming situation (Buli´c et al. 2012), and a minimal representation of troposphere-stratosphere interactions (Herceg-Bulic et al. 2018, Ruggieri et al. 2017).

The source code and the documentation of the current version of the model - including information on model development and subsequent releases, can be found at http://users.ictp.it/~kucharsk/speedy-net.html.

2.2 Experimental setup

Considering that the goal of the analysis is to assess the sensitivity of the ENSO-related teleconnections to different model mean states, an initial step is to produce several "SPEEDY worlds", characterized by different mean climates. Considering the geographical position of the ENSO thermal forcing, changes in the model mean states are obtained by modifying the average structure of the Pacific jet stream. A simple but effective approach is to change the orography over the Rocky Mountains region. Indeed, the Rockies play a relevant role in shaping and modulating the Northern Hemisphere climate (e.g., White et al, 2021), weakening the zonal wind, strengthening the stationary wave pattern and producing a southwest-northeast tilt of the Atlantic eddy-driven jet. These effects are due to the peculiar topography of the Rocky Mountains, which generates a dipole with an anticyclone on the windward and poleward side of the mountain range (where the wind has to "go over" the mountain) and a cyclone on the leeward and equatorward side (where the flow is more effectively blocked so that is partially diverted around the mountain) (Brayshaw et al, 2009). By modulating the height of the Rocky Mountains, it is possible to modify the jet interaction with the orographic obstacle and thus change the mean flow over both the Pacific and the Atlantic sector.

2.2.1 Changes to the Rocky Mountains

2.2.1.1 Control Simulation (ROCK-0) A 200-year long control climate simulation run using the SPEEDY default configuration is used as a baseline experiment (hereafter named ROCK-0). The SST and the Sea Ice Concentration (SIC) boundary conditions are obtained from the 1979–2008 monthly climatology from the European Centre for Medium-Range Weather Forecasts re-analysis (ERA-Interim; Dee et al. 2011). Daily SST and SIC forcing data are obtained by linearly interpolating monthly mean values. In order to reduce the model internal variability, the sea ice and the land modules are switched off. The radiative parameters are set to represent values of the last decades of the 20th century (King et al. 2010). Model integration starts with a standard atmosphere at rest in hydrostatic equilibrium.

2.2.1.2 Modified orography experiments (ROCK) Twelve 200-year long simulations are performed with a set of modified orographies to obtain different mean states of the mid-latitude atmospheric circulation. The twelve modified orography simulations are characterized by an increased or decreased height of the Rocky Mountains in a box spanning 170 W-90 W and 10-80 N. The North American orography

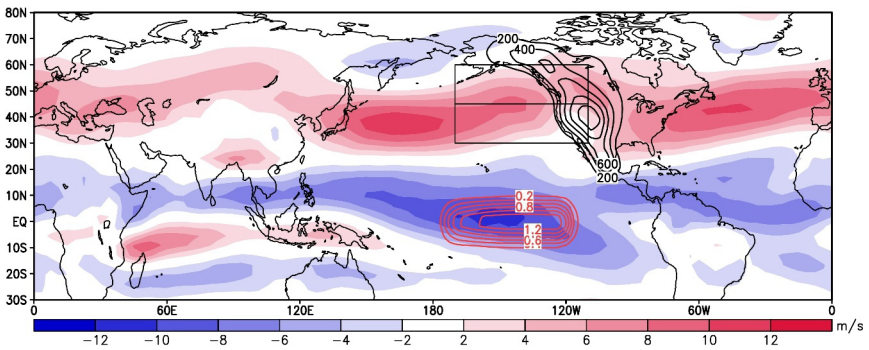

Fig. 2 JFM climatology of the zonal wind at 850 hPa for the ROCK-0 simulation (colours). Black boxes are the regions where the PJS and PJL indices are calculated (see text for details). The black contours show the difference between the ROCK + 60 and ROCK-0 orography (units: m). The red contours in the equatorial Pacific show the intensity of the idealised El Niño SST anomaly (units: K)

is referred to as Rocky Mountains because, due to its resolution, the SPEEDY model is unable to resolve smaller mountain chains as Sierra Nevada and the Cascades. The changes to the height of the Rocky Mountains ranges from − 60% to + 60% (-60%, -50%, -40%, -30%, -20%, -10%, + 10%, + 20%, + 30%, + 40%, + 50% and + 60%). In order to avoid discontinuities in the orography field along the edge of the box, a nine grid point smoothing is applied at the borders of the domain. The twelve simulations with changes in the height of the Rocky Mountains, together with the ROCK-0 control simulation, are hereafter named ROCK experiments. Figure 2 shows an example of a 60% increase of the height of the Rocky Mountains (ROCK + 60 experiment). The last three characters in the name of the experiments indicate the percentage change in the height of the Rocky Mountains.

By comparing ROCK experiments with modified orography and ROCK-0, the effectiveness of the orography in producing changes in the mean state of the Pacific jet stream is assessed.

2.2.2 Idealized tropical forcing (ENSO forcing)

To study the impact of the model bias on the response to external forcing, four sets of ENSO-like simulations are conducted. The SST pattern of an idealized ENSO anomaly, both positive (El Niño) and negative (La Niña), is defined in the El Niño 3.4 region (Equatorial Pacific Ocean, 5 N-5 S, 170 W-120 W): this anomaly is then superimposed to the climatological SST for all the orographic configurations of the ROCK experiments. The shape and magnitude of the idealized anomaly in the El Niño case are generated as follows:

- from HadSST3 data (1979 to 2008, see Kennedy et al. 2011b, 2011c), all El Niño events are extracted detecting events for which the 5-month running mean of the monthly SST anomalies in the El Nino 3.4 region are greater than 0.5 K for six consecutive months or more (for the El Niño 3.4 index, see Trenberth, 1997).
- The SST composite of the above-defined events is computed over the El Niño 3.4 region. For each event the (6) monthly anomalies are taken. The composite is made by the average of the considered monthly anomalies.
- A nine-grid-point smoothing is applied along the edges of the area.
- This idealized El Niño3.4 anomaly is finally superimposed on the climatological SST.

The red contours in Fig. 2 show the area and the intensity of the selected idealized El Niño3.4 anomaly. Two sets of experiments are then designed, for both El Niño and La Niña phases. The first set of experiments is conducted with the idealized El Niño3.4 anomaly just described (a "standard intensity" El Niño), which has a maximum of about 1.2 K (NINO experiments hereafter). The experiment with El Niño forcing and no orographic change is thus labelled NINO-0. The second set of experiments uses the same anomaly pattern, but doubled in magnitude (i.e., NINOx2 experiments). The experiment with twice El Niño forcing and no orographic change is named NINOx2-0. Following the same methodology, the La Niña and the La Niña with doubled idealized anomalies are obtained by reversing the sign of the El Niño experiments (defined as NINA and NINAx2 experiments). Similarly, the experiments with no orographic change, are labelled NINA-0 and NINAx2-0, respectively.

Since the ENSO signal is stronger during the late boreal winter, i.e., January-March (JFM) (Brönnimann 2007, King et al. 2021), the analysis is limited to this season.

Similarly to the ROCK experiments, the NINO, NINOx2, NINA, and NINAx2 integrations are 200-year long. All the simulations start from an atmosphere at rest and in order to discard the spin-up of the model, the first year of each integration is excluded.

By comparing ENSO experiments (NINO, NINOx2, NINA, NINAx2) and the corresponding ROCK simulations it is possible to estimate the modulation of the ENSO signal due to the change of the model mean state.

This idealized configuration has strengths and limitations; on the one hand, the idealized SST forcing helps to understand the mechanism behind the interaction between the bias of the Pacific Jet stream and the ENSO response, isolating the source of the signal over the Central Pacific. On the other hand, the observed ENSO SST signal is characterized by anomalies outside the Niño3.4 region that might generate non-negligible signals and non-linear interactions with the signals coming from the Niño3.4 region.

2.2.3 Reanalysis and fully fledged general circulation models

To provide an estimate of the SPEEDY biases in the ROCK and ENSO experiments the ECMWF ERA-Interim Reanalysis (1979–2018) is used. The El Niño signal is obtained by compositing the geopotential height field during the El Niño events (in the 1979–2018 period) identified with the Nino3.4 index. The reference for state-of-the-art general circulation models is the Coupled Model Intercomparison Project phase 6 (CMIP6, Eyring et al. 2016): considering the atmosphere-only setup of the SPEEDY integrations, the focus is on the Atmospheric Model Intercomparison Project experiment (AMIP, Gates et al. 1998). AMIP simulations are performed over the historical period 1979–2014, with observed sea surface temperature and sea-ice and observed

greenhouse gases (GHGs) and stratospheric ozone mixing ratios and aerosol emissions. Because models have different resolutions, all the model outputs are interpolated to a 2.5°x2.5° regular lat-lon grid[1].

2.3 Metrics

Considering the relevance for this study of the propagation of the ENSO signal from the tropics to the extratropics, the position of the so-called "Pacific Waveguide" is of key importance (Dawson et al. 2011). The Rossby stationary waveguide is strictly related to three parameters characterizing the jet stream: (1) the jet strength, (2) the latitudinal position of the jet maximum and (3) the jet width (Manola et al. 2013). In order to characterize the mean state of each ROCK simulation, two dynamical indices that define such properties of the Pacific jet stream are introduced. A Pacific Jet Strength index (PJS) and a Pacific Jet Latitude index (PJL):

- the PJS index is the average of the 850 hPa zonal wind in a box spanning 110-170 W and 30-60 N, and it is used to measure the intensity of the Pacific jet stream;
- the PJL index is the average of the 850 hPa zonal wind in a box 110-170 W and 45-60 N minus the same average in a box 110-170 W and 30-45 N. The PJL index aims at describing the latitudinal position (and therefore the associated meridional wind shear) of the Pacific jet stream.

The jet width has been investigated as well. This is estimated as the distance between the inflection points of the meridional profile of the zonally averaged zonal wind at 850 hPa (between 110 and 170 W, Manola et al. 2013). Our results show that the jet width exhibits a large variability and its estimate is affected by a large uncertainty, and changes in the orography have a weak (if not null) effect on it (see supplementary material figure SM1), so this property is not further discussed.

The box used for the computations is shown in Fig. 2.

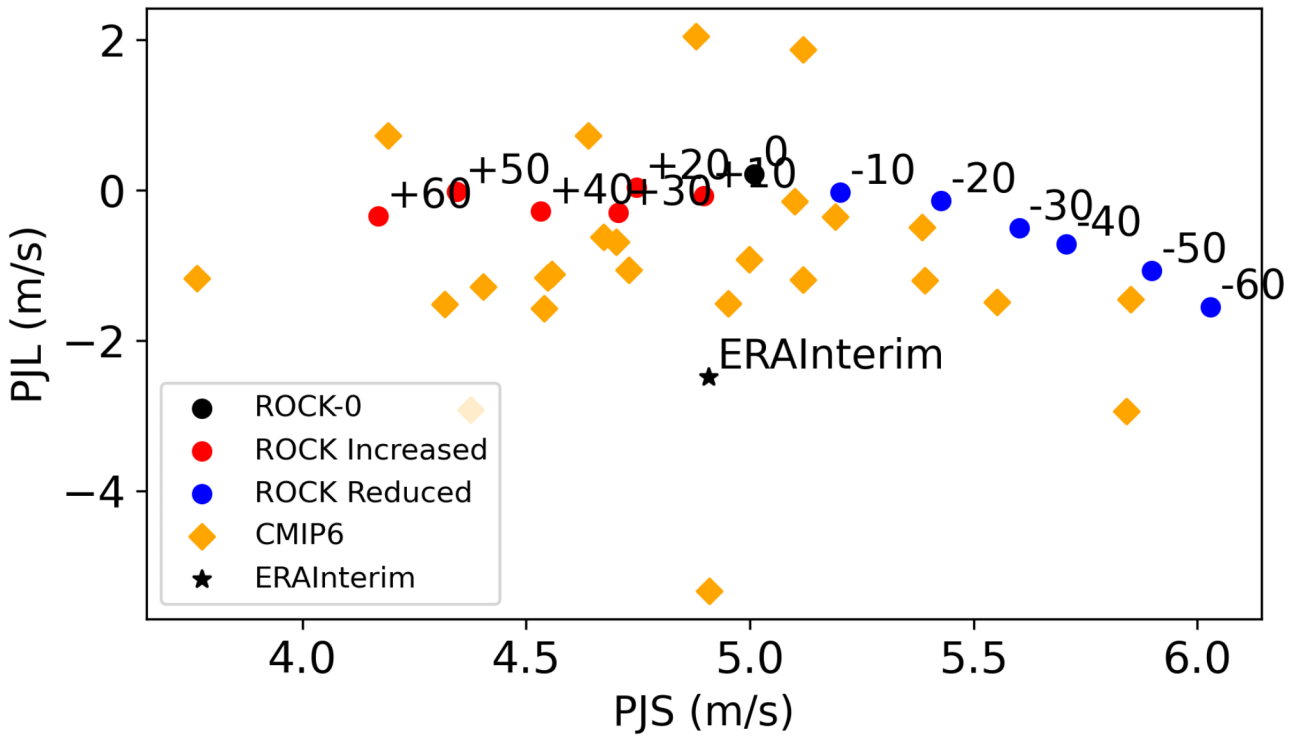

Fig. 3 JFM PJL index vs. PJS index. Orange diamonds are models from CMIP6, blue dots are ROCK experiments with reduced orography, red dots are ROCK experiments with increased orography. Black dot is the ROCK-0 experiment and the black star is ERA-Interim

[1] List of CMIP6 models used: ACCESS-CM2, ACCESS-ESM1-5, BCC-CSM2-MR, BCC-ESM1, CAMS-CSM1-0, CanESM5, CAS-ESM2-0, CESM2, CESM2-FV2. CESM2-WACCM, CESM2-WACCM-FV2, CIESM, EC-Earth3, EC-Earth3-Veg, FGOALS-f3-L, FGOALS-g3, FIO-ESM-2-0, GFDL-ESM4, INM-CM4-8, INM-CM5-0, IPSL-CM6A-LR, MIROC6, MPI-ESM2-0, NorESM2-LM.

The PJS and PJL indices are calculated at 850 hPa because at this level the effect of changes in the orography is more evident than in the upper troposphere. However, indices calculated using the zonal wind at 300 hPa exhibit a similar behaviour (see supplementary material figure SM2).

3 Results

3.1 The mean state

To understand how the Pacific jet stream changes in the ROCK experiments (e.g., from ROCK-60 to ROCK + 60) and how these changes are related with the mean climate of state-of-the-art GCMs, the two indices (PJS and PJL) calculated from the ROCK simulations are compared with the same indices computed from CMIP6.

Figure 3 shows a scatterplot with the PJS index against the PJL index for the CMIP6 (orange diamonds) and SPEEDY (blue and red dots) experiments, all compared to ERA-Interim (the black star). All models show a relevant bias in the PJL index with respect to reanalysis, having a Pacific jet always displaced too poleward. On the other hand, PJS indices from CMIP6 models and ROCK experiments are scattered around the value from the reanalysis; the PJS values range from 4 to 6. The ROCK experiments cover approximately a fair amount of the CMIP6 model spread in terms of the PJS index. As expected, the more the Rockies are lowered, the stronger the Pacific jet becomes. Conversely, the changes in the height of the Rocky Mountains have a moderate and non-linear impact on the values of the PJL index. While the latitude of the jet is slightly affected by the increase of the orography, the PJL index decreases linearly for lower orography: indeed, a larger negative value of the PJL index implies an equatorward displacement of the Pacific jet.

Figure 4 shows the impact of Rocky Mountains orography changes on the zonal wind at 850 hPa for the JFM season, which is mainly found over the North American continent and the North Pacific basin, with a secondary structure over the North Atlantic and Eurasia. As expected from Fig. 3, the ROCK-60 experiment (Fig. 4a) is characterized by a stronger jet. The signal in the zonal wind is maximum over the mountains, and spreads mainly upstream up to the center of the Pacific Ocean. The ROCK + 60 experiment (Fig. 4c) shows an opposite behaviour, with the effect of the orography localized only on the region of the Rockies and downstream, over the North American continent.

The linear regression in Fig. 4b, all the average JFM fields from ROCK experiments are merged together into a single array and then the linear regression is calculated, shows the relation between the lower-tropospheric zonal wind and the PJS: a stronger Pacific jet is associated with an intensified zonal wind over the Rocky Mountains in a latitude band between 30 and 50 N. At latitudes southern than 30 N a stronger Pacific jet reinforces the trade winds. In a latitudinal band between 50 and 70 N, the response of the zonal wind reverts; here a stronger Pacific jet weakens the local zonal wind. A smaller but significant signal is found over the tropical Atlantic Ocean (60 W-0 W) and in the mid-latitudes of the Euro-Asiatic sector, where the zonal wind strengthens with a more intense Pacific jet.

3.2 SPEEDY response to idealized ENSO

In order to show the response to an idealized ENSO in the Pacific-Western North American sector, the JFM 500 hPa geopotential height is considered (King et al. 2017, Feng et al. 2017, Alexander et al. 2008). Figure 5 shows the response to an idealized El Niño in the 500 hPa geopotential height for the NINO-0 (Fig. 5b) and ERA-Interim (Fig. 5a). In the Pacific and the North American sectors, the response in the geopotential height due to the idealized El Niño SST

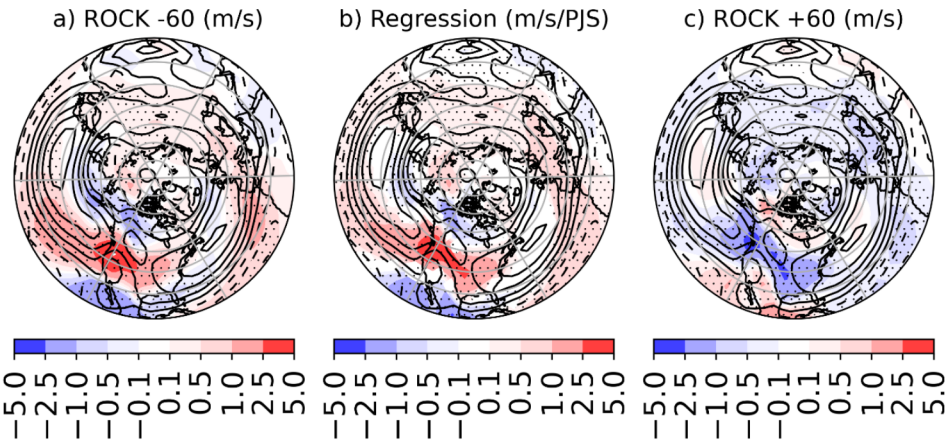

Fig. 4 JFM 850 hPa zonal wind (m/s). (a,c) Differences between the modified orography experiments (ROCK-60 and ROCK + 60) and ROCK-0 (shading). (b) linear regression of the zonal wind from all ROCK experiments on the PJS index. Contours are the full field from the ROCK-0. Stippling shows regions where the values are statistically significant (two tailed t-test, $\alpha = 0.05$)

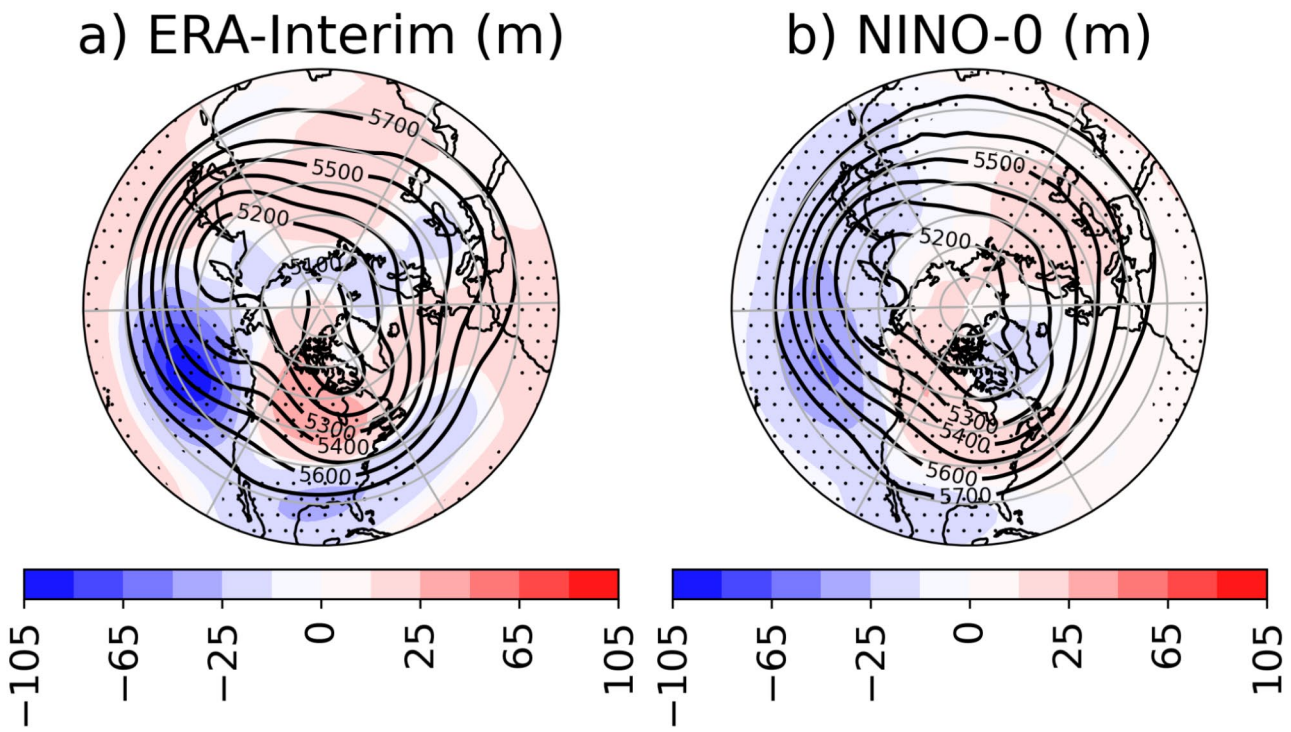

Fig. 5 JFM response to El Niño in geopotential height at 500 hPa for ERA-Interim (a) and SPEEDY (NINO-0 minus ROCK-0,b). Contours are the respective climatological geopotential height and colours are the responses to El Niño. Stippling shows regions where the signals are statistically significant (two tailed t-test, $\alpha = 0.05$)

is in good agreement with observations (e.g., Horel and Wallace 1981, Bracco et al. 2007, Kucharski et al. 2007, Rodriguez-Fonseca et al. 2009, Kröger and Kucharski 2011, Bulić et al. 2012, Wang 2017, Dogar et al. 2017, Mezzina et al. 2019). The NINO-0 response shows a strong negative anomaly in the Pacific Ocean (120E-120 W, 30-50 N) and a positive anomaly over the North American continent (180-110 W, 50-80 N). These two anomalies, combined with the (weaker) negative anomaly over Mexico, constitute the typical Rossby wave train associated with ENSO. Another negative anomaly is found over Greenland.

The response to an idealized La Niña (NINA-0 experiment, see supplementary material) shows a signal characterized by a positive anomaly over the Pacific Ocean, a negative anomaly over the North American continent and positive anomaly over Mexico, consistent with the Rossby wave train for La Niña. The NINA-0 experiment also shows a significant positive signal over the Atlantic Ocean.

Overall, the NINO-0 run shows a westward displaced Rossby wave train and weaker positive pole when compared to ERA-Interim. It is worth noting that the observed North Atlantic pole of the Rossby wave train is missing in the NINO-0 experiment, suggesting a weaker atmospheric bridge between the two basins in SPEEDY. However, over Europe and the Middle East, the reanalysis and the NINO-0 experiment show similar patterns; both show a positive anomaly of about 10 m. Conversely, Eastern Asia and Japan are regions where the NINO-0 experiment and ERA-Interim are more in contrast: in the NINO-0 experiment, the negative anomaly in the Pacific Ocean elongates westward till reaching Japan and the coasts of Asia, while in ERA-Interim a positive anomaly over Asia and Japan is observed. Considering the idealized framework of the NINO experiments, a discrepancy between SPEEDY and ERA-Interim is expected. Nonetheless, the overall response is in satisfactory agreement with respect to the reanalysis.

The NINA-0 experiment, compared with ERA-Interim, shows an overall weaker signal with respect to ERA-Interim (See Supplementary Material Fig.SM7). In SPEEDY, the Rossby wave train, starting from the Pacific Ocean and crossing the North American continent is roughly the half of the signal observed in the reanalysis. The only exception is the positive pole over Mexico, which is comparable with ERA-Interim. The positive centre of action on the Pacific Ocean is shifted to the west with respect to the reanalysis and covers all the ocean up to Japan.

The asymmetry of the signals between El Niño and La Niña are caused by the different impact that imposing a warm or cold SST anomaly on the climatological SST might have. Indeed, small warm SST anomalies over the tropical

western Pacific can enhance convection and induce large rainfall anomalies. Conversely, for cold SST anomalies over the tropical eastern Pacific, strong SST anomalies are

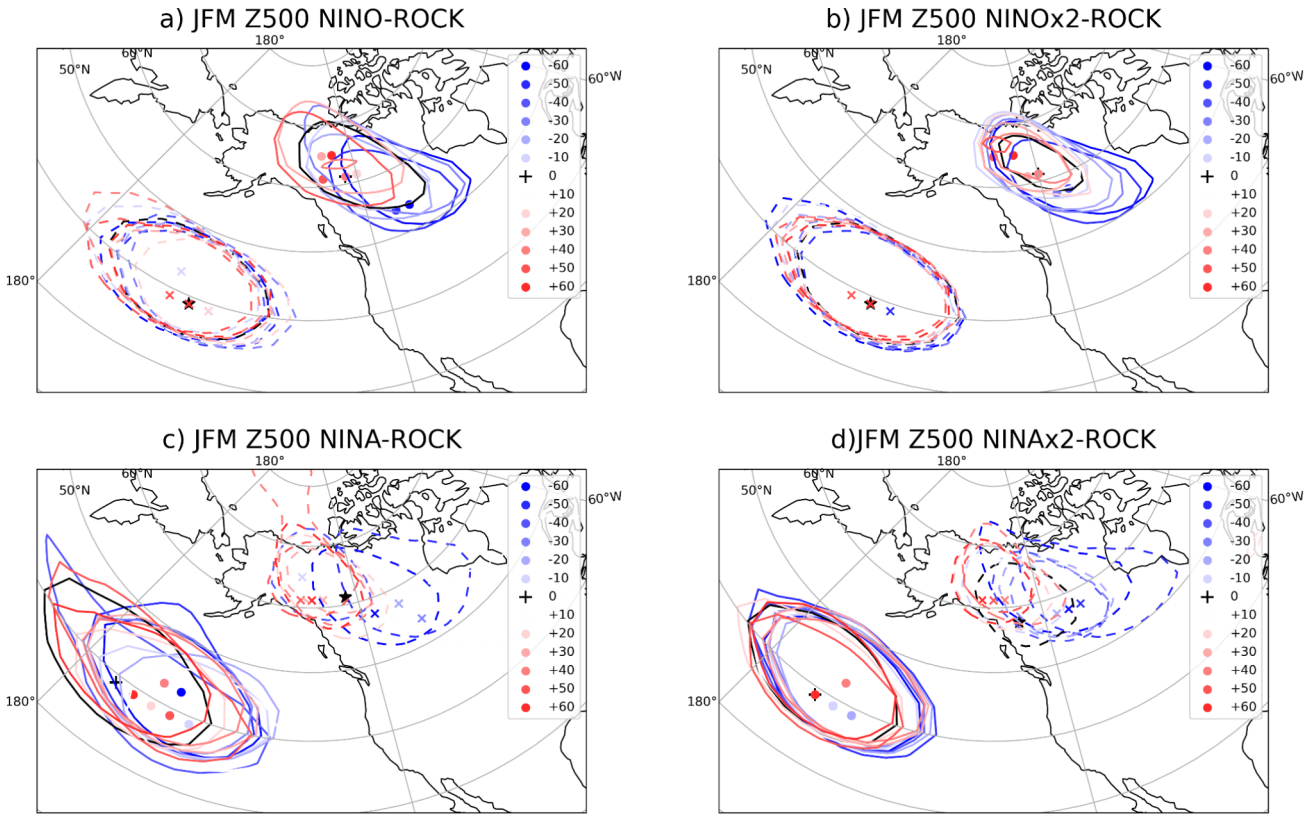

Fig. 6 JFM dipole response to ENSO in the geopotential height at 500 hPa for (a) for NINO-ROCK experiments (b) for NINOx2-ROCK experiments, (c) for NINA-ROCK experiments, and (d) for NINAx2-ROCK experiments. Only one contour for the North Pacific anomaly and only one for North America anomaly are drawn. Contours are chosen arbitrarily in order to highlight displacement of the anomaly. Dots show the positions of the maximum positive response and crosses the position of the minimum negative response. The value for the anomaly over the North American continent for the NINA experiments is about − 9 m, while the same for NINO reaches 15 m. Similarly, NINAx2 shows a maximum signal of about − 17 m, while NINOx2 gets up to 30 m

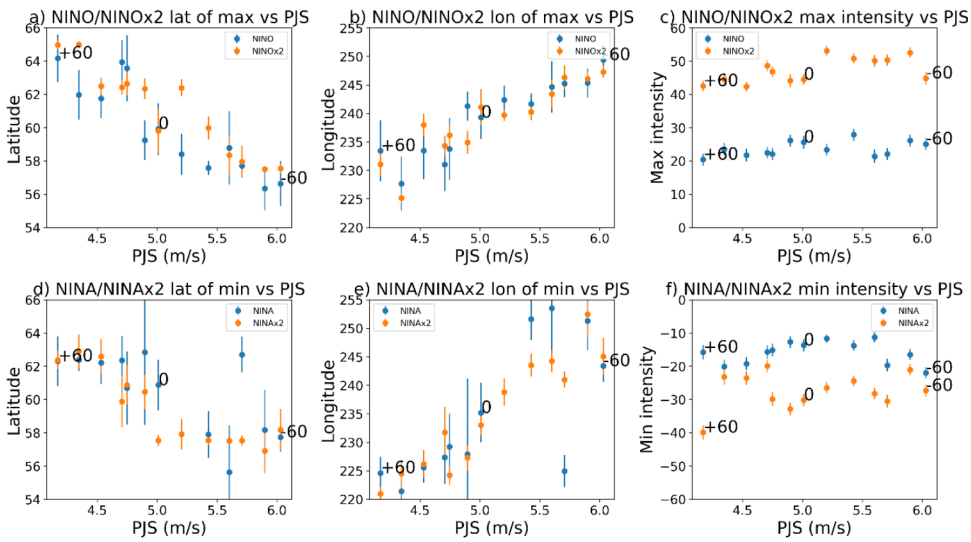

Fig. 7 JFM 500 hPa geopotential height response to NINO, NINA, NINOx2, and NINAx2 for all ROCK experiments. (a) NINO and NINOx2 latitude of the maximum of the response. (b) NINO and NINOx2 longitude of the maximum of the response. (c) NINO and NINOx2 geopotential height intensity of the maximum of the response. (d,e,f) are the same as (a,b,c) but for the minimum of the response in NINA and NINAx2 experiments. In all the panels the mean is represented by a dot and the standard deviation by the vertical bars

required to induce the convective anomalies (Timmermann et al. 2018).

3.3 NIN*-ROCK experiments

To study the relationship between the model bias and the ENSO response in the different NINO (NINA) and NINOx2 (NINAx2) experiments, the properties of the geopotential height dipole over the Pacific Ocean and North America (i.e., the ENSO Rossby wave train) are investigated.

This is done, for each experiment, by looking at the geographical position of the maximum (minimum) over the North America and the North Pacific poles (i.e., in the case of an El Niño response anomaly, this corresponds to a positive pole over North America and a negative pole over the North Pacific). Results are shown in Fig. 6: while the position of the signal over the ocean is weakly affected by orographic changes, the position of the signal over North America (see dots for El Niño and crosses for La Niña) migrates along a south-east/north-west axis as long as the height of the Rockies is increased.

Although a significant change is seen for the position, the intensity of the ENSO Rossby wave train is not affected by the height of orography. The magnitude of the signal doubles when the intensity of the forcing is doubled (e.g., NINO vs. NINOx2). On the other hand, a strong nonlinearity in the ENSO teleconnection is observed when NINO and NINA experiments are compared. The El Niño signal is almost twice the intensity than its La Niña counterpart.

A graphical summary of these results is provided by Fig. 7, where the latitude, longitude, and intensity of the maximum (minimum) of the geopotential height at 500 hPa over North America for all the idealized ENSO NINO (NINA) and NINOx2 (NINAx2) experiments are shown.

In order to provide an estimate of the uncertainty in the position of the maxima/minima over the North America region due to internal variability, a bootstrap method is used. From the 200-year simulation, 130 JFM seasons (63% of the data, as suggested by Efron and Tibshirani 1993) are randomly chosen and averaged. Then the position of the maxima/minima of the geopotential height at 500 hPa in the box [45-70 N, 150 W-90 W] is computed. The sampling is repeated 3000 times. In this way, it is possible to estimate the uncertainty of the position of the maximum/minimum, denoted in the figure by the extension of the bars, which shows the standard deviation of the bootstrap sample. By increasing the intensity of the Pacific jet (i.e. by reducing the height of the Rockies) the center of action of the response over North America moves from north-west to south-east (Fig. 7a,b,d,e). On the other hand, the intensity of the North American response does not change as the intensity of the Pacific jet increases (Fig. 7c,f). Results are consistent for all sets of NINO, NINOx2, NINA and NINAx2 experiments. However, a minor difference can be noted: the standard deviation of the position (for both the longitude and latitude) of the positive PNA pole decreases when the intensity of the idealised El Niño anomaly is doubled. This suggests that, not surprisingly, a stronger forcing provides a larger signal-to-noise ratio.

The same bootstrap approach is applied to the signal over the Pacific Ocean (see supplementary material Fig. SM6). When looking at the position of the pole over the ocean of the ENSO Rossby wave train, it is found that there is no significant shift in its latitudinal and longitudinal position and the intensity of the anomaly doesn't change.

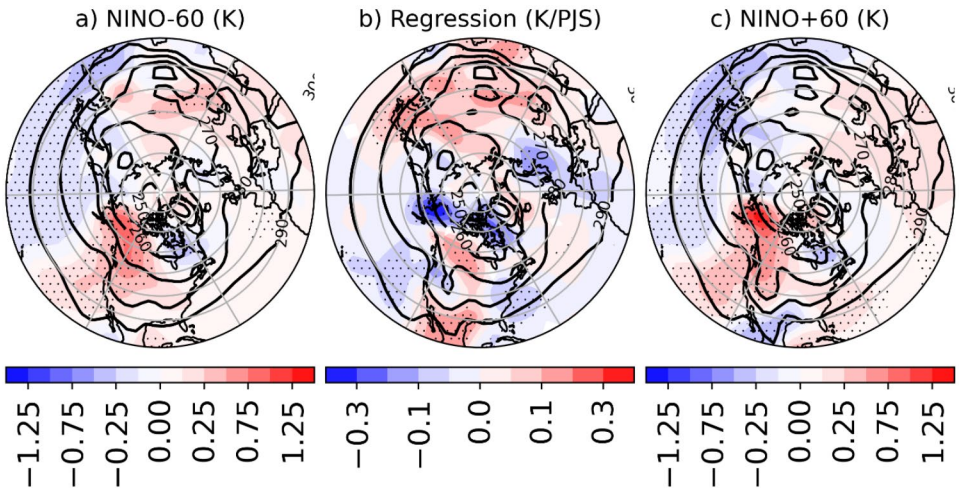

Fig. 8 JFM near surface air temperature response in NINO experiments (NINO - ROCK). (b) Linear regression between the near surface air temperature and the PJS index. (a,c) Two examples of the changes in the response to El Niño (NINO-60 and NINO + 60). Stipplings show regions where the values are significant (FDR, $\alpha_{global} = 0.20$, Wilks, 2006). Contours show the near surface air temperature of the relative baseline experiments: (a) ROCK-60, (b) ROCK-0 and (c) ROCK + 60

3.4 Implications for modelled impacts of ENSO

To better assess the sensitivity of the ENSO-induced teleconnection patterns to the model mean state, the responses of near surface air temperature and total precipitation are analyzed. Almost the same patterns - but with doubled amplitude - are obtained from NINOx2 experiments (not shown). Conversely, NINA and NINAx2 experiments show approximately opposite impacts (not shown).

The Northern Hemisphere near surface air temperature response (Fig. 8a,c) shows that El Niño has wide but moderate impacts all over the Northern Hemisphere, with near surface air temperature changes not larger than +/- 0.5 K. The only region where El Niño has a stronger signal is Western North America. A clear warm signal is present over Alaska and Canada, where the near surface air temperature increases by 1.25 K. The same anomaly, reduced in intensity, also extends southward over the West coast of the United States. While experiments with the increased orography (Fig. 8c) show a negative temperature anomaly over Mexico, those with reduced orography (Fig. 8a) are characterized by a neutral or positive response.

Another clear signal is located over Japan: a cold anomaly spreads downstream, from the Asian East coast to the Pacific Ocean. On the other hand, the signal over Europe, North Africa, and the Arabian Peninsula (a warm anomaly unaffected by changes of the mean state) is weak and becomes statistically significant only in the NINOx2 experiments.

The linear regression shown in Fig. 8b, which shows the relationship between the ENSO near surface air temperature response and the PJS Index, highlights the role of the changes in the mean state in modifying the ENSO temperature fingerprint. The response over Western Alaska is weakened when the PJS index increases, implying that a stronger jet tends to suppress the warm signal there. Similarly, in Mexico the cold signal of the response decreases as the PJS index increases, but the sign changes when the PJS index exceeds a threshold value.

On the contrary, the positive signal over Canada is enhanced by a stronger Pacific jet. The response over Asia resembles the one over Mexico, but only the responses over Japan and the Middle East seem to be significantly affected by the mean state, and both become colder when the intensity of the jet stream over the Pacific Ocean decreases. To summarize, larger PJS indices (i.e., for stronger jet speeds) strengthen the zonal flow. This leads to a more zonal configuration of the Rossby wave train to the idealized ENSO-like SST anomaly and a reduction of the meridional advection. As a consequence, a reduction in the intensity of the temperature anomaly is observed. The temperature anomaly reduces over most of the Northern Hemisphere. Two minor exceptions, where the temperature anomaly is enhanced, are Canada and the region east of the Caspian Sea.

Figure 9 shows the total precipitation response for NINO experiments. As expected, the pattern of precipitation anomaly produced by NINO experiments shows a marked signal over tropical regions. The total precipitation shows the typical equatorial El Niño signal, with an increase in the eastern and central Equatorial Pacific (not shown), while it decreases in tropical and subtropical regions approximately corresponding to the downward branch of the Hadley cell.

A positive rainfall response is also located near the California coast and the Aleutian region, extending further upstream in the Pacific Ocean. A second positive rainfall response is in the Gulf of Mexico, Florida, and Caribbean region, whose signal also extends over Mexico and reaches the eastern tropical Pacific. On the other hand, El Niño favours a decrease in precipitation over India, Southeast Asia, and Japan.

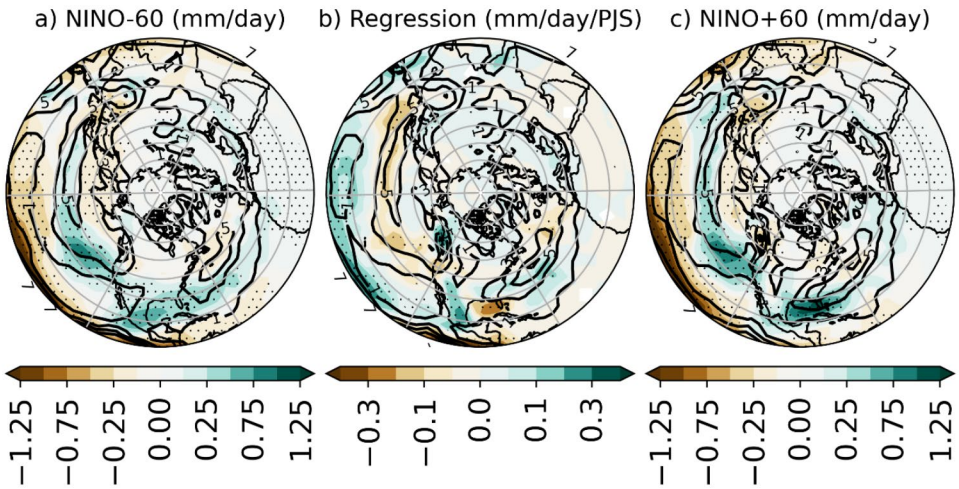

Fig. 9 As Fig. 8, but for precipitation

The regression of the total precipitation on the PJS index (Fig. 9b) shows modulation of the signal following a change in the mean state over multiple regions: the most relevant signal is a dipolar anomaly that involves Caribbeans and Mexico. Over the Caribbean, the total precipitation decreases when the PJS index increases, with NINO experiments showing a stronger relationship between the signal and the PJS index. Conversely, the total precipitation over Mexico increases with the PJS index.

Similarly, the tropical Pacific is strongly affected by the Pacific Jet stream intensity, and the total precipitation regression shows an increase in the precipitation greater than 0.30 mm/day/m/s. The response on the west coast of Canada on the border with Alaska shows an increase of the precipitation associated with an increase of the Pacific Jet intensity, while an opposite signal is observed over the Aleutian low.

3.5 Rossby waves propagation and the Rossby stationary wavenumber

The above-described sensitivity of the ENSO response (Fig. 6) can be investigated in terms of the linear theory of Rossby wave propagation (Hoskins and Karoli 1981). Rossby waves are planetary-scale waves that propagate westward with respect to the time-averaged background flow so that they can become stationary if the mean westerly flow presents the opportune conditions; they are capable of transferring energy and momentum across large distances and giving rise to teleconnection patterns (Hoskins and Karoli 1981). Rossby waves can be generated by diabatic heating, a condition which typically occurs in areas of deep convection at tropical latitudes: consequently, anomalous Rossby waves can be produced following the onset of ENSO. The way Rossby waves propagate in a slowly varying flow is well understood; Rossby stationary waves tend to be refracted towards regions with larger stationary wavenumber (K_s), usually equatorward (Hoskins and Ambrizzi 1993). Rossby stationary waves and the stationary wavenumber can be compared, respectively, to a light beam and the refractive index in optics.

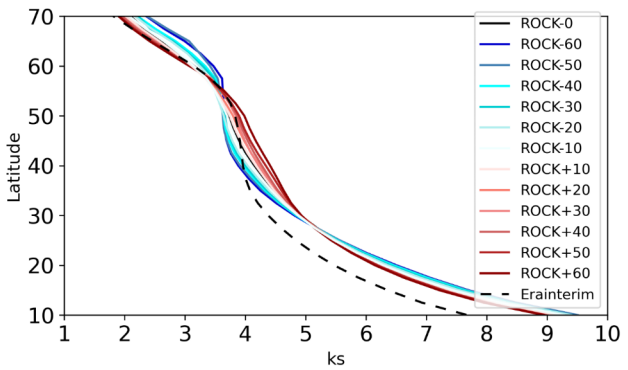

Fig. 10 JFM meridional profile of Rossby stationary wavenumber at 300 hPa. K_s is calculated by averaging the zonal wind at 300 hPa over a region between 170-110 W. The black dashed line represents ERA-Interim, the black line is the ROCK-0 simulation, reds are ROCK experiments with increased orography, and blues ROCK experiments with reduced orography

K_s is defined as follows:

$$K_s = \sqrt{k^2 + l^2} = (\beta_M / u_M)^{1/2}$$

where k is the zonal wavenumber, l is the meridional wavenumber, β is $cos(\Phi)$ times the meridional gradient of the absolute vorticity, and u is the zonal velocity. The subscript M indicates the Mercator projection on the sphere. From the kinematic wave theory, given a Rossby stationary wave characterized by a fixed K_s, the zonal wavenumber k is constant along the Rossby wave path, so the meridional wavenumber l has to vary, and this change in l is the reason for the variation in the propagation direction. The propagation of the Rossby wave in the meridional direction is stopped when the wave reaches a latitude characterized by a meridional wavenumber equal to zero ($l = 0$); the group velocity becomes purely zonal, so the wave is refracted back to lower latitudes. Latitudes characterized by $l = 0$ are usually called "turning latitudes".

The presence of a zonal jet affects the propagation of Rossby waves. The intensity and the width of the midlatitude jet are two key properties to create an effective waveguide that can propagate the Rossby wave along the zonal direction (Manola et al. 2013).

The turning latitude can be computed from the meridional profile of *Ks*. Given a meridional profile of $K_s(\phi)$ and a stationary Rossby wave characterized by a zonal wavenumber n, the turning latitude is the latitude where the function $K_s(\phi)$ crosses the vertical line $n = const$. In our case, the meridional profile of the stationary wavenumber is calculated by zonally averaging the zonal wind over the Pacific sector (170 W-110 W) and considering only the Northern Hemisphere (10-70 N). The longitudinal size of the Pacific sector is comparable with the typical scale of quasi-stationary Rossby waves (Scaife et al. 2017).

Figure 10 shows the meridional profile for each ROCK experiment and for the ERA-Interim: Red curves refer to ROCK experiments with increased Rocky Mountains height, blue curves refer to ROCK experiments with reduced height, the solid black line corresponds to the ROCK-0 experiment, while the dashed black line to the ERA-Interim reanalysis. For wavenumbers greater than 4 it can be noticed that the ERA-Interim reanalysis shows a constantly lower turning latitude than ROCK experiments. For values between 3 and 4, the range of values computed from

the ROCK experiments is comparable with the reanalysis values. Nonetheless, the meridional profile is different and none of the SPEEDY experiments is able to represent the reanalysis profile well. For values lower than 3, the spread of the ROCK experiment is reduced and all the simulations satisfactorily follow the profile of ERA-Interim. The experiments with the larger Rocky Mountains, however, are more similar to the reanalysis than those with the Rocky Mountains decreased, possibly because the higher orographic barrier reduces the jet speed reducing the zonal wind model bias. Moreover, Fig. 3 showed that ERA-Interim has a lower value of the PJL index with respect to the ROCK experiments. The bias in the latitudinal position of the jet stream is related to the bias in the meridional profile of the Rossby stationary wavenumber. Indeed, a jet at lower latitudes implies lower turning latitudes.

It is evident how the turning latitude associated with wavenumbers between 3 and 5, which correspond to the typical Rossby signal generated by ENSO (Li et al. 2020) changes with the height of the Rocky Mountains and consequently with the speed and the position of the Pacific jet. Experiments characterized by a more intense jet stream over the Pacific Ocean (blue lines) show equatorward turning latitudes; experiments with a weaker jet stream show poleward turning latitudes. The changes of the turning latitude values across ROCK experiments are consistent with the observed changes of the position of the ENSO-induced Rossby wave train over North America in NINO/NINA experiments (Fig. 7); a stronger jet modifies the propagation of Rossby waves reducing the values of the turning latitude and thus inducing a southward shift of the signal in geopotential height. On the other hand, a weaker jet leads to a poleward turning latitude and a consequent poleward shift of the Rossby wave train.

4 Discussion

Not many authors have explored the impact of changes in models' orography. Generally, the most used approach is either the complete removal of the orography or the removal of a specific mountain chain (White et al. 2017,2018, Baldwin et al. 2021). For example, several papers studied the role of the Tibetan plateau and the Mongolian mountains (Boos & Kuang 2010, Chiang et al. 2015, Shi et al. 2016, White et al. 2017, Kong & Chiang 2020) in shaping the large-scale Northern Hemisphere atmospheric circulation. White et al. 2021 compared simulations with standard orography and simulations carried out removing completely all the orography. They found out that the orography reduces the mean zonal wind by 50–80% and, without the orography, the wintertime zonal wind of the Northern Hemisphere is comparable with the Southern Hemisphere winter jet. The resolved orography accounts for about 1/3 of the total slowdown of zonal wind. The ROCK experiments, which showed (Figs. 3 and 4) that the height of the Rocky Mountains affects linearly the zonal wind, are consistent with these results.

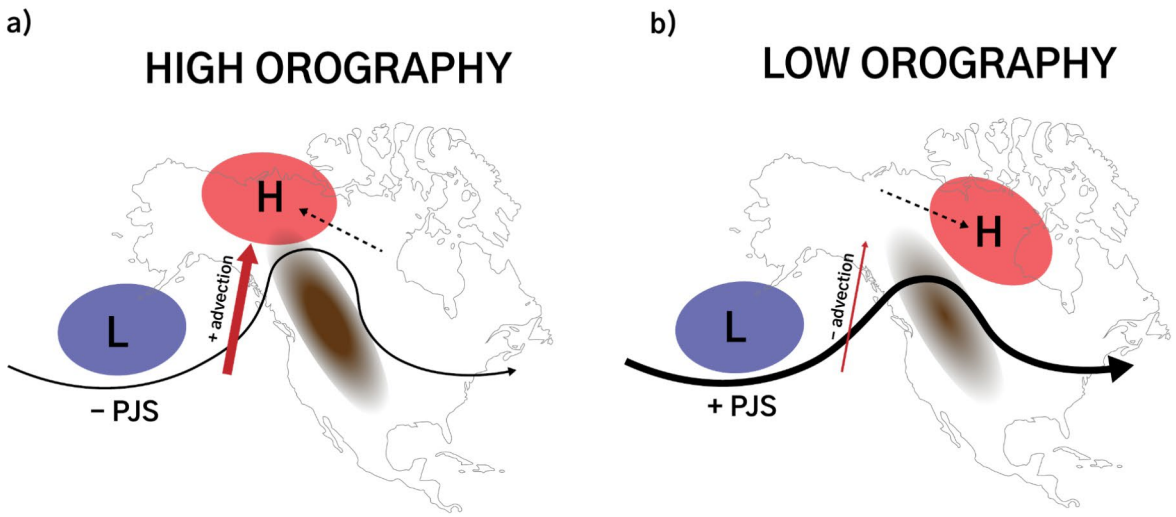

Fig. 11 Schematic representation of the impact of the orography on the ENSO response

The idealized ENSO experiments are similar to experiments carried out in previous works. In particular, Dogar et al. 2017 (here on D17) performed four ENSO experiments using the SPEEDY model: two El Niño and two La Niña experiments with regular and doubled intensity respectively. They used a SST anomaly imposed on the climatology, only in the tropical region (50 S-50 N). Given the very similar structure of this and D17 experiments, a direct comparison is possible. Despite the differences in the ENSO forcing (full Tropical Pacific in D17 and Niño3.4 region in this work), the near-surface temperature in D17 four ENSO experiments is similar. The west coast of the North American continent shows the typical positive (negative) signal related to an El Niño (La Niña) event. The intensities of the near-surface temperature anomalies are comparable to our NINO-0(NINA-0) and NINOx2-0(NINAx2-0) experiments. In D17 the responses in near-surface temperature extend over the Hudson Bay, while in our experiments the anomalies are confined in the west of Hudson Bay. These differences highlight the importance of the SST in the Tropical Pacific outside of the Niño3.4 region. The Extratropical North Pacific Ocean shows a very consistent response in the two works. The spatial pattern and intensity of the total precipitation response found in our experiments match well D17 results.

The schematic shown in Fig. 11 summarises the mechanism behind the modulation of the ENSO signal by orography over North America. An increased orography (panel on the left) reduces the intensity of the Pacific jet in the exit region over the continent. The reduction of the zonal component of the wind is associated with an increased meridional component of the wind and more advection of warm air from the tropics to mid-latitudes. This can be interpreted as the air having not enough kinetic energy to go over the orographic barrier and being deviated poleward. Lastly, the high-pressure anomaly (due to El Niño) is displaced to the North-West. On the other hand, a reduced orography (panel on the right) increases the jet strength in the exit region and reduces the meridional component of the wind, resulting in a more zonal jet. Consequently, the meridional advection is reduced so that less warm air reaches the higher latitudes. The positive center of action over the continent migrates to the South-East.

The results and the interpretation of the link between the ENSO response over the North American continent and the atmospheric mean state (i.e., the zonal wind) proposed in this work are supported by Benassi et al. (2021). They explore the impact of low-frequency SST variability over the extratropical Pacific on the El Niño teleconnection, concluding that different values of the zonal wind in the jet exit region over North America can modulate the response to ENSO. As in this study, they found that a weaker jet leads to a more poleward ENSO wave train.

Similarly, it has been shown that the position and intensity of the ENSO centre of action in the geopotential height at 500 hPa over the Pacific do not change with different mean states: this confirms the work of Tyrrell and Karpechko (2021), who found that changes in the model zonal wind bias do not affect the ENSO signal in the Aleutian Low.

5 Summary and conclusions

This work aims at investigating the role of the mean atmospheric state, and in particular by the North Pacific zonal flow mean state, in modulating the atmospheric response to ENSO and its impacts on temperature and total precipitation. A set of experiments is developed in order to modify the mean state of the SPEEDY intermediate complexity general circulation model via progressively increasing or decreasing the height of the Rocky Mountains. Each experiment is forced with the same idealized ENSO SST anomaly. Finally, linear Rossby waves propagation theory is used to interpret the results.

SPEEDY experiments show that, by changing the height of the Rocky Mountains, it is possible to modify the mean state of the model over the North Pacific sector. Indeed, it is shown that the speed of the Pacific jet changes comparably to the zonal wind-speed bias of state-of-the-art global climate models. Comparison with the values of the same Pacific Jet indices computed for the CMIP6 models indicates that the SPEEDY experiments are able to mimic the bias in the Pacific jet strength of CMIP6 models (Fig. 3).

The midlatitude leading response to El Niño is a geopotential height anomaly over the North Pacific and North America, stronger during the late winter and reminiscent of the PNA pattern (King et al. 2018). In the SPEEDY experiments, the Rossby wave train in response to a tropical El-Niño-like forcing is clearly affected by changes in the mean state. When the Pacific jet is stronger (i.e., when the Rocky Mountains height is reduced), the positive geopotential height response center over Canada and Alaska migrates from north-west to south-east. The position of the center of action of the 500 hPa geopotential height response of the idealized El Niño experiments moves about 4° southward and about 10° longitude eastward following an increase of the jet speed of about 1 m/s. For idealized La Niña experiments, the position of the center of action moves about 2° southward and 14° longitude eastward with an increase of the jet speed of about 1 m/s. Responses to the double intensity idealized El Niño and La Niña experiments are roughly the same as the regular intensity experiments.

More generally, the observed sensitivity of the ENSO-induced Rossby wave train can be interpreted in terms of linear Rossby Wave propagation theory. Experiments with a stronger jet over the North Pacific are characterized by an average turning latitude, for wavenumbers from 3 to 5, located at lower latitudes than experiments with a weaker jet. The difference in the turning latitudes directly influences the direction of propagation of Rossby waves: experiments with a weaker jet show that the Rossby Wave train is shifted westward and northward, while experiments with a stronger jet tend to confine Rossby waves to lower latitudes and enhance a f "waveguide" effect. The final result is that larger Pacific jet speed favours an eastward and equatorward shift of the Rossby Wave train, with a more zonally oriented propagation. Interestingly, the SPEEDY experiments show that the strength of the Pacific jet does not affect the intensity of the response to an idealized ENSO anomaly, but only its position.

Due to the different characteristics of the Pacific jet, the propagation of the tropically generated Rossby waves changes accordingly, leading to different global teleconnections. For instance, a stronger Pacific jet is associated with a less intense surface temperature response over Alaska: the signal of the idealized El Niño experiments decreases by about 0.4 K following an increase of 1 m/s in the wind intensity. The Pacific jet strength also affects the dipolar signal of total precipitation over the Caribbean and Mexico regions: the intensity of the NINO experiments responses decrease (increase) over the Caribbean (Mexico) by about 0.3 mm/day following an increase of 1 m/s of the jet speed. Another way to look at the role of the bias of the Pacific jet is by considering that a stronger jet-speed strengthens the zonal flow. The increased zonal flow leads to a more zonal configuration of the Rossby wave train to the idealized ENSO forcing and the consequence is a reduction of the meridional advection over the North American region. The position of the centers of action of the geopotential height signal induces a reduction of the temperature anomaly intensity over Alaska and a shift of the total precipitation pattern over Mexico and the Caribbean.

Overall, this work showed that the model mean state (or, in other words, model systematic error) can affect the mid-latitude response to tropical forcing. Different intensities of the Pacific jet lead to different propagations of Rossby waves and different ENSO responses across the North American continent.

The comparison between SPEEDY and CMIP6 GCM behaviour proves that SPEEDY experiments have the capability to mimic the bias of the CMIP6 models with respect to the importance of a good representation of the Pacific jet stream. Experiments with ENSO show the key role of model bias in signal propagation from the tropics to mid-latitudes. This confirms the great importance of reducing the bias in the zonal wind of state-of-the-art models in order to increase their ability to describe the essential dynamical processes of general circulation. SPEEDY results pave the way for several future works focusing on the relationship between Pacific jet misrepresentation and response to external forcing in state-of-the-art GCM models.

Supplementary Information The online version contains supplementary material available at https://doi.org/10.1007/s00382-022-06261-w.

References

Ayarzagüena B, Ineson S, Dunstone NJ, Baldwin MP, Scaife AA (2018) Intraseasonal Effects of El Niño–Southern Oscillation on North Atlantic Climate, Journal of Climate, 31(21), 8861–8873. Retrieved Dec 9, 2021, from https://journals.ametsoc.org/view/journals/clim/31/21/jcli-d-18-0097.1.xml

Alexander M, Scott J (2008) The Role of Ekman Ocean Heat Transport in the Northern Hemisphere Response to ENSO. J Clim - J Clim 21:5688–5707. https://doi.org/10.1175/2008JCLI2382.1

Baldwin JW, Atwood AR, Vecchi GA, Battisti DS (2021) Outsize influence of Central American orography on global climate. AGU Advances, 2, e2020AV000343. https://doi.org/10.1029/2020AV000343

Bayr T, Wengel C, Latif M et al (2019a) Error compensation of ENSO atmospheric feedbacks in climate models and its influence on simulated ENSO dynamics. Clim Dyn 53:155–172. https://doi.org/10.1007/s00382-018-4575-7

Bayr T, Domeisen DIV, Wengel C (2019b) The effect of the equatorial Pacific cold SST bias on simulated ENSO teleconnections to the North Pacific and California. Clim Dyn 53:3771–3789. https://doi.org/10.1007/s00382-019-04746-9

Benassi M, Conti G, Gualdi S et al (2021) El Niño teleconnection to the Euro-Mediterranean late-winter: the role of extra-tropical Pacific modulation. Clim Dyn. https://doi.org/10.1007/s00382-021-05768-y

Blade I (1999) The influence of midlatitude ocean–atmosphere coupling on the low-frequency variability of a GCM. Part II: interannual variability induced by tropical SST forcing. J Clim 12:21–45

Boos WR, Kuang Z (2010) Dominant control of the South Asian monsoon by orographic insulation versus plateau heating. Nature 463(7278):218–222. https://doi.org/10.1038/nature08707

Bourke W, Formulation I, Integrations H (1974)Monthly Weather Review, 102(10),687–701. Retrieved Jan 25, 2021, from https://journals.ametsoc.org/view/journals/

mwre/102/10/1520-0493_1974_102_0687_amlsmi_2_0_co_2.xml
Bracco A, Kucharski F, Molteni F et al (2007) A recipe for simulating the interannual variability of the Asian summer monsoon and its relation with ENSO. Clim Dyn 28:441–460. https://doi.org/10.1007/s00382-006-0190-0
Brayshaw DJ, Hoskins B, Blackburn M (2009) The Basic Ingredients of the North Atlantic Storm Track. Part I: Land–Sea Contrast and Orography, Journal of the Atmospheric Sciences, 66(9), 2539–2558. Retrieved Feb 4, 2021, from https://journals.ametsoc.org/view/journals/atsc/66/9/2009jas3078.1.xml
Brönnimann S (2007) Impact of El Niño–Southern Oscillation on European climate. Rev Geophys 45:RG3003. https://doi.org/10.1029/2006RG000199/
Bulić IH, Brankovi´c ˇC, Kucharski F (2012) Winter ENSO teleconnections in a warmer climate. Clim Dyn 38(7–8):1593–1613
Butler Amy H, Polvani Lorenzo M, Deser Clara (2014) Separating the stratospheric and tropospheric pathways of El Niño–Southern Oscillation teleconnections. Environ Res Lett 9(2): 024014. IOP Publishing
Cagnazzo C, Manzini E (2009) Impact of the Stratosphere on the Winter Tropospheric Teleconnections between ENSO and the North Atlantic and European Region, Journal of Climate, 22(5), 1223–1238. Retrieved May 12, 2021, from https://journals.ametsoc.org/view/journals/clim/22/5/2008jcli2549.1.xml
Chang EKM (2013) CMIP5 projection of significant reduction in extratropical cyclone activity over North America. J Clim 26(24):9903–9922
Chiang JCH, Fung IY, Wu C-H, Cai Y, Edman JP, Liu Y et al (2015) Role of seasonal transitions and westerly jets in East Asian paleoclimate. Q Sci Rev 108:111–129. https://doi.org/10.1016/j.quascirev.2014.11.009
Claussen M, Mysak L, Weaver A et al (2002) Earth system models of intermediate complexity: closing the gap in the spectrum of climate system models. Clim Dyn 18:579–586. https://doi.org/10.1007/s00382-001-0200-1
Dai A, Wigley TML (2000) Global patterns of ENSOinduced precipitation. Geophys Res Lett 27:1283–1286. https://doi.org/10.1029/1999GL011140
Dawson A, Matthews AJ, Stevens DP (2011) Rossby wave dynamics of the North Pacific extra-tropical response to El Niño: importance of the basic state in coupled GCMs. Clim Dyn 37:391–405. https://doi.org/10.1007/s00382-010-0854-7/
Dee DP, Uppala SM, Simmons AJ, Berrisford P, Poli P, Kobayashi S, Andrae U, Balmaseda MA, Balsamo G, Bauer P, Bechtold P, Beljaars ACM, van de Berg L, Bidlot J, Bormann N, Delsol C, Dragani R, Fuentes M, Geer AJ, Haimberger L, Healy SB, Hersbach H, Hólm EV, Isaksen L, Kållberg P, Köhler M, Matricardi M, McNally AP, Monge-Sanz BM, Morcrette J-J, Park B-K, Peubey C, de Rosnay P, Tavolato C, Thépaut J-N, Vitart F (2011) The ERA-Interim reanalysis: configuration and performance of the data assimilation system. Q J R Meteorol Soc 137:553–597. https://doi.org/10.1002/qj.828
Dogar MM, Kucharski F, Azharuddin S (2017) Study of the global and regional climatic impacts of ENSO magnitude using SPEEDY AGCM. J Earth Syst Sci 126:30. https://doi.org/10.1007/s12040-017-0804-4
Domeisen DI, Garfinkel CI, Butler AH (2019) The teleconnection of El Niño Southern Oscillation to the stratosphere. Rev Geophys 57:5–47. https://doi.org/10.1029/2018RG000596
Domeisen DIV, Butler AH, Fröhlich K, Bittner M, Müller WA, Baehr J (2015) Seasonal Predictability over Europe Arising from El Niño and Stratospheric Variability in the MPI-ESM Seasonal Prediction System. J Clim 28(1):256–271 Retrieved Dec 10, 2021, from. https://journals.ametsoc.org/view/journals/clim/28/1/jcli-d-14-00207.1.xml
Eyring V, Bony S, Meehl GA, Senior CA, Stevens B, Stouffer RJ, Taylor KE (2016) Overview of the Coupled Model Intercomparison Project Phase 6 (CMIP6) experimental design and organization. Geosci Model Dev 9:1937–1958. https://doi.org/10.5194/gmd-9-1937-2016
Feng J, Chen W, Li Y (2017) Asymmetry of the winter extra-tropical teleconnections in the Northern Hemisphere associated with two types of ENSO. Clim Dyn 48:2135–2151. https://doi.org/10.1007/s00382-016-3196-2
Gates WL, Boyle J, Covey C, Dease C, Doutriaux C, Drach R, Fiorino M, Gleckler P, Hnilo J, Marlais S, Phillips T, Potter G, Santer B, Sperber K, Taylor K, Williams D (1998) An Overview of the Results of the Atmospheric Model Intercomparison Project (AMIP I). Bull Amer Meteor Soc 73:1962–1970
Gershunov A, Cayan D (2003) Heavy daily precipitation frequency over the contiguous United States: sources of climate variability and seasonal predictability. J Clim 16:2752–2765. https://doi.org/10.1175/1520-0442 (2003)016%3C275 2:HDPFO T%3E2.0.CO;2
Harvey BJ, Cook P, Shaffrey LC, Schiemann R (2020) The response of the northern hemisphere storm tracks and jet streams to climate change in the CMIP3, CMIP5, and CMIP6 climate models. J Geophys Research: Atmos 125:e2020JD032701. https://doi.org/10.1029/2020JD032701
Held IM, Suarez MJ (1994) A Proposal for the Intercomparison of the Dynamical Cores of Atmospheric General Circulation Models. Bull Am Meteorol Soc 75(10):1825–1830 Retrieved Jan 25, 2021, from. https://journals.ametsoc.org/view/journals/bams/75/10/1520-0477_1994_075_1825_apftio_2_0_co_2.xml
Brian HOSKINS, AMBRIZZI J, Tercio (1993) Rossby wave propagation on a realistic longitudinally varying flow. J Atmos Sci 50(12):1661–1671
Brian HOSKINS, KAROLY J, David J (1981) The steady linear response of a spherical atmosphere to thermal and orographic forcing. J Atmos Sci 38(6):1179–1196
Jiménez–Esteve B, Domeisen DIV (2018) The tropospheric pathway of the ENSO–North Atlantic teleconnection. J Clim 31(11):4563–4584. doi:https://doi.org/10.1175/JCLI-D-17-0716.1
Kennedy JJ, Rayner NA, Smith RO, Saunby M, Parker DE (2011b) Reassessing biases and other uncertainties in sea-surface temperature observations since 1850 part 1: measurement and sampling errors. J Geophys Res 116:D14103. doi:https://doi.org/10.1029/2010JD015218
Kennedy JJ, Rayner NA, Smith RO, Saunby M, Parker DE (2011c) Reassessing biases and other uncertainties in sea-surface temperature observations since 1850 part 2: biases and homogenisation. J Geophys Res 116:D14104. doi:https://doi.org/10.1029/2010JD015220
King MP, Kucharski F, Molteni F (2010) The Roles of External Forcings and Internal Variabilities in the Northern Hemisphere Atmospheric Circulation Change from the 1960s to the 1990s, Journal of Climate, 23(23), 6200–6220. Retrieved Jul 26, 2021, from https://journals.ametsoc.org/view/journals/clim/23/23/2010jcli3239.1.xml
King MP et al (2018) "Interannual tropical Pacific sea surface temperature anomalies teleconnection to Northern Hemisphere atmosphere in November". Clim Dyn 50(5):1881–1899
King MP, Herceg-Bulić I, Bladé I, García-Serrano J, Keenlyside N, Kucharski F, Li C, Sobolowski S (2018) Importance of Late Fall ENSO Teleconnection in the Euro-Atlantic Sector. Bull Am Meteorol Soc 99(7):1337–1343 Retrieved May 28, 2021, from. https://journals.ametsoc.org/view/journals/bams/99/7/bams-d-17-0020.1.xml
King MP, Li C, Sobolowski S (2021) Resampling of ENSO teleconnections: accounting for cold season evolution reduces uncertainty in

the North Atlantic. Weather and Climate Dynamics Discussions, pp 1–24
Kong W, Chiang JC (2020) Interaction of the westerlies with the Tibetan Plateau in determining the mei-yu termination. J Clim 33(1):339–363. https://doi.org/10.1175/jcli-d-19-0319.1
Kröger J, Kucharski F (2011) Sensitivity of ENSO characteristics to a new interactive flux correction scheme in a coupled GCM. Clim Dyn 36:119–137. https://doi.org/10.1007/s00382-010-0759-5
Kucharski F, Molteni F, Bracco A (2006a) Decadal interactions between the western tropical Pacific and the North Atlantic oscillation. Clim Dyn 26(1):79–91
Kucharski F, Molteni F, Yoo JH (2006b) SST forcing of decadal Indian monsoon rainfall variability. Geophys Res Lett 33(3). doi: https://doi.org/10.1029/2005GL025371
Kucharski F, Bracco A, Yoo JH, Molteni F (2007) Low-frequency variability of the Indian monsoon–ENSO relationship and the tropical Atlantic: The 'weakening' of the 1980s and 1990s. J Clim 20(16):4255–4266
Kucharski F, Zeng N, Kalnay E (2013a) A further assessment of vegetation feedback on decadal Sahel rainfall variability. Clim Dyn 40(5–6):1453–1466
Kucharski F, Molteni F, King MP, Farneti R, Kang IS, Feudale L 2013b On the need of intermediate complexity general circulation models: A 'SPEEDY' example;Bull. Am. Meteorol. Soc.94(1)25–30
Lau N-C (1997) Interactions between global SST anomalies and the midlatitude atmospheric circulation. Bull Am Meteor Soc 78:21–33
Li, Ronald KK et al (2020) Effect of the North Pacific tropospheric waveguide on the fidelity of model El Niño teleconnections. J Clim 33(12):5223–5237
Lopez H, Kirtman BP (2019) ENSO influence over the Pacific North American sector: uncertainty due to atmospheric internal variability. Clim Dyn 52:6149–6172. https://doi.org/10.1007/s00382-018-4500-0
Manola I, Selten F, de Vries H, Hazeleger W (2013) "Waveguidability" of idealized jets. J Geophys Res Atmos 118(432– 10,440). doi:https://doi.org/10.1002/jgrd.50758
Meehl GA, Covey C, Taylor KE, Delworth T, Stouffer RJ, Latif M, McAvaney B, Mitchell JF (2007) The WCRP CMIP3 multimodel dataset: A new era in climate change research. Bull Amer Meteor Soc 88:1383–1394. https://doi.org/10.1175/BAMS-88-9-1383
Mezzina B, García-Serrano J, Bladé I, Kucharski F (2020) Dynamics of the ENSO Teleconnection and NAO Variability in the North Atlantic–European Late Winter, Journal of Climate, 33(3), 907–923. Retrieved Aug 5, 2021, from https://journals.ametsoc.org/view/journals/clim/33/3/jcli-d-19-0192.1.xml
Mizuta R (2012) Intensification of extratropical cyclones associated with the polar jet change in the CMIP5 global warming projections. Geophys Res Lett 39:19
Molteni F, Ferranti L, Palmer TN, Viterbo P (1993) A dynamical interpretation of the global response to equatorial Pacific SST anomalies. J Clim 6:777–795
Molteni F (2003) Atmospheric simulations using a GCM with simplified physical parametrizations. I. Model climatology and variability in multi-decadal experiments. Clim Dyn 20:175–191
Molteni F, King MP, Kucharski F, Straus DM (2011) Planetary-scale variability in the northern winter and the impact of land–sea thermal contrast. Clim Dyn 37(1–2):151–170
Moron V, Gouirand I (2003) Seasonal modulation of the El Niño–southern oscillation relationship with sea level pressure anomalies over the North Atlantic in October–March 1873–1996. Int J Climatol 23:143–155. https://doi.org/10.1002/joc.868
Palmer TN (1999) A nonlinear dynamical perspective on climate prediction. J Clim 12:575–591
Philander SG, Wang C (1990) (2018). A review of ENSO theories. Natl. Sci. Rev. 5, 813–825. doi:https://doi.org/10.1093/nsr/nwy104
Rodríguez-Fonseca B, Polo I, García-Serrano J, Losada T, Mohino E, Mechoso CR, Kucharski F (2009) Are Atlantic Niños enhancing Pacific ENSO events in recent decades? Geophys Res Lett 36:L20705. doi:https://doi.org/10.1029/2009GL040048
Ruggieri P, Kucharski F, Buizza R, Ambaum MHP (2017) The transient atmospheric response to a reduction of sea-ice cover in the Barents and Kara Seas. Q J R Meteorol Soc 143(704):1632–1640
Scaife AA, Comer RE, Dunstone NJ, Knight JR, Smith DM, MacLachlan C, Martin N, Peterson KA, Rowlands D, Carroll EB, Belcher S, Slingo J (2017) Tropical rainfall, Rossby waves and regional winter climate predictions. Q J R Meteorol Soc 143:1–11. https://doi.org/10.1002/qj.2910
Seager R, Harnik N, Robinson WA, Kushnir Y, Ting M, Huang HP, Velez J (2005a) Mechanisms of ENSO-forcing of hemispherically symmetric precipitation variability. Q J R Meteorol Soc 131:1501–1527
Seager R, Kushnir Y, Herweijer C, Naik N, Velez J (2005b) Modeling of tropical forcing of persistent droughts and pluvials over western North America: 1856–2000. J Clim 18:4065–4088
Shi Z, Sha Y, Liu X (2016) Effect of Yunnan–Guizhou Topography at the Southeastern Tibetan Plateau on the Indian Monsoon. J Clim 30(4):1259–1272. https://doi.org/10.1175/JCLI-D-16-0105.1
Straus DM, Shukla J (2002) Does ENSO force the PNA? J Clim 15:2340–2358
Taylor KE, Stouffer RJ, Meehl GA (2012) An Overview of Cmip5 and the Experiment Design. Bull Am Meteorol Soc 93(4):485–498
Tibshirani RJ (1993) "An introduction to the bootstrap. Monogr Stat Appl Probab 57:1–436
Timmermann A, An SI, Kug JS et al (2018) El Niño–Southern Oscillation complexity. Nature 559:535–545. https://doi.org/10.1038/s41586-018-0252-6
Trenberth KE (1997) The Definition of El Niño, Bulletin of the American Meteorological Society, 78(12), 2771–2778. Retrieved Feb 9, 2021, from https://journals.ametsoc.org/view/journals/bams/78/12/1520-0477_1997_078_2771_tdoeno_2_0_co_2.xml
Trenberth KE, Branstator GW, Karoly D, Kumar A, Lau N, Ropelewski C (1998) Progress during TOGA in understanding and modeling global teleconnections associated with tropical sea surface temperatures. J Geophys Res 103:14 291–14324. https://doi.org/10.1029/97JC01444
Tyrrell NL, Karpechko AYu (2020) Minimal impact of model biases on northern hemisphere ENSO teleconnections, Weather Clim. Dynam Discuss [preprint]. https://doi.org/10.5194/wcd-2020-59
Ulbrich U, Leckebusch GC, Joaquim G (2009) Pinto. "Extra-tropical cyclones in the present and future climate: a review. Theoret Appl Climatol 96(1):117–131
Wallace JM (1981) Gutzler. "Teleconnections in the geopotential height field during the Northern Hemisphere winter. Mon Weather Rev 109(4):784–812
Wang C, Deser C, Yu JY, DiNezio P, Clement A (2017) El Niño and Southern Oscillation (ENSO): A Review. In: Glynn P, Manzello D, Enochs I (eds) Coral Reefs of the Eastern Tropical Pacific. Coral Reefs of the World, vol 8. Springer, Dordrecht. https://doi.org/10.1007/978-94-017-7499-4_4
White RH, Wallace JM, Battisti DS (2021) Revisiting the Role of Mountains in the Northern Hemisphere Winter Atmospheric Circulation, Journal of the Atmospheric Sciences (published online ahead of print 2021). Retrieved Jun 7, 2021, from https://journals.ametsoc.org/view/journals/atsc/aop/JAS-D-20-0300.1/JAS-D-20-0300.1.xml
Wilks DS (2006) On "Field Significance" and the False Discovery Rate. J Appl Meteorol Climatology 45(9):1181–1189 Retrieved

Dec 17, 2021, from. https://journals.ametsoc.org/view/journals/apme/45/9/jam2404.1.xml
Zappa G, Shaffrey LC, Kevin I (2013) Hodges. "The ability of CMIP5 models to simulate North Atlantic extratropical cyclones. J Clim 26(15):5379–5396
Wilks, D. S. (2006). On "Field Significance" and the False Discovery Rate, Journal of Applied Meteorology and Climatology, 45(9), 1181–1189. Retrieved Dec 17, 2021, from https://journals.ametsoc.org/view/journals/apme/45/9/jam2404.1.xml
Zappa, Giuseppe, Len C. Shaffrey, and Kevin I. Hodges. "The ability of CMIP5 models to simulate North Atlantic extratropical cyclones." Journal of Climate 26.15 (2013): 5379–5396.